Modified Skyhook Control of Semi-Active Suspensions: A New Model, Gain Scheduling, and Hardware-in-the-Loop Tuning

Keum-Shik Hong
School of Mechanical Engineering
e-mail: kshong@hyowon.pusan.ac.kr

Hyun-Chul Sohn
Department of Mechanical and Intelligent Systems Engineering
e-mail: hcson@hyowon.pusan.ac.kr

Pusan National University,
30 Changjeon-dong, Kumjeong-ku,
Pusan 609-735, Korea

J. Karl Hedrick
Department of Mechanical Engineering,
University of California Berkeley,
Berkeley, CA 94720-1740
e-mail: khedrick@me.berkeley.edu

In this paper, a road adaptive modified skyhook control for the semi-active Macpherson strut suspension system of hydraulic type is investigated. A new control-oriented model, which incorporates the rotational motion of the unsprung mass, is introduced. The control law extends the conventional skyhook-groundhook control scheme and schedules its gains for various road conditions. Using the vertical acceleration data measured, the road conditions are estimated by using the linearized new model developed. Two filters for estimating the absolute velocity of the sprung mass and the relative velocity in the rattle space are also designed. The hydraulic semi-active actuator dynamics are incorporated in the hardware-in-the-loop tuning stage of the control algorithm developed. The optimal gains for the ISO road classes are discussed. Experimental results are included. [DOI: 10.1115/1.1434265]

Keywords: Macpherson Strut Suspension, Modeling, Skyhook Control, Semi-Active Damper, Gain Scheduling, Rapid Control Prototyping, Road Estimation

1 Introduction

The roles of a suspension system are to support the vehicle weight, to isolate the vehicle body from road disturbances, and to maintain the traction force between the tire and the road surface. Suspension systems are classified into a passive system and an active system according to the existence of control input. The active suspension system can be further classified into two types: a semi-active system and a fully active system according to the control input generation mechanism. The semi-active suspension system uses a varying damping force as a control force. For example, a hydraulic semi-active damper varies the size of an orifice in the hydraulic flow valve to generate desired damping forces. An electro-rheological (ER) damper or a magneto-rheological (MR) damper applies various levels of electric field or magnetic field to cause various viscosities of the ER or MR fluids. On the other hand, the fully active suspension system produces the control force with a separate hydraulic/pneumatic unit. Therefore, the cost and the weight of a fully active suspension system are much higher than those of a semi-active one. Semi-active suspension systems are getting more attention because of their low cost and competitive performance to the fully active ones. In this paper, a road adaptive modified skyhook control for the semi-active Macpherson strut suspension system of hydraulic type is investigated.

The performance of a suspension system is characterized by the ride quality, the handling performance of vehicle, the size of the rattle space, and the dynamic tire force. The prime purpose of adopting an active/semi-active suspension system is to improve the ride quality and the handling performance of vehicle. To improve the ride quality, it is important to isolate the sprung mass from the road disturbances and to suppress the vertical vibrations near 5 Hz (4–8 Hz), which is known to be a sensitive frequency range to human body (lateral vibrations at 1–2 Hz) according to ISO 2631. On the other hand, to improve the handling performance of vehicle, it is important to keep the tire in contact with the road surface and therefore to decrease the resonant peak near 10 Hz, which is the resonant frequency of the unsprung mass. For a fixed suspension spring constant, the better isolation of the sprung mass from the road disturbances can be achieved with a soft damping by allowing a larger suspension deflection. However, the better road contact can be achieved with a hard damping by not allowing unnecessary suspension deflections. Therefore, the ride quality and the handling performance of vehicle are two conflicting criteria in the control system design of suspension systems.

Since the skyhook control strategy was introduced by Karnopp et al. [1], in which a fictitious damper is inserted between the sprung mass and the stationary sky as a way of suppressing the vibratory motion of the sprung mass and as a tool to compute the desired damping force, a number of innovative control methodologies have been proposed to implement this strategy. The skyhook control can reduce the resonant peak of the sprung mass quite significantly and thus achieves a good ride quality. But, in order to improve both the ride quality and the handling performance of vehicle, both resonant peaks of the sprung mass and the unsprung mass need to be reduced. It is known, however, that the skyhook damper alone cannot reduce both resonant peaks at the same time. From this point of view, Besinger et al. [2] proposed a modification of the skyhook control, which includes both a passive damper as well as a skyhook damper, for the computation of desired control inputs. Novak and Valasek [3] have proposed a groundhook control, which assumes an additional fictitious damper between the unsprung mass and the ground, for the purpose of decreasing the dynamic tire force.

Compared to the various control techniques appeared in the literature, the issues related to the modeling of suspension systems are rare. Jonsson [4] conducted a finite element analysis for evaluating the deformations of suspension components. Stensson et al. [5] proposed three nonlinear models for the Macpherson strut wheel suspension for the analysis of motion, force, and deformations. These models would be appropriate for the analysis of mechanics, but are not adequate for control purpose. In the conventional quarter car model (Yue et al. [6]), only the up-down movements of the sprung and unsprung masses are assumed. In the conventional model, the role of the control arm is completely

Contributed by the Dynamic Systems and Control Division for publication in the JOURNAL OF DYNAMIC SYSTEMS, MEASUREMENT, AND CONTROL. Manuscript received by the Dynamic Systems and Control Division May 1, 2000. Associate Editor: S. Sivashankar.

ignored. From this point of view, a new control-oriented model, which includes the rotational motion of the control arm, is introduced.

As an actuator for generating the semi-active control force, a continuously variable damper (CVD) is used. Hence, the control force is adjusted by changing the size of an orifice of the CVD. The damping force characteristics of a CVD are highly nonlinear. Also, the CVD used in this work is designed in such a way that it produces much larger damping force in the extension motion than in the compression motion. It is also noted that with a semi-active suspension the control action is applied only when the control force is opposite to the direction of suspension relative velocity.

One way of designing a control system for the semi-active suspension is to figure out all the nonlinearities of the plant and actuator and then to design an appropriate control law based upon both the vehicle dynamics and the actuator dynamics. For this, the fluid dynamics of the variable damper has to be investigated. However, it is not simple to know the complete nonlinear characteristics of the variable damper. Also, considering the fact that the entire control problem is to stabilize a multiple-degree underactuated mechanical system with one saturating actuator in the presence of unknown road disturbances, see Fig. 3 for control problem formulation, the efforts to know the complete nonlinear dynamics of the actuator is not so cost-effective.

Another way is to isolate the most significant nonlinear part of the actuator, which is the variable damper in our case, and to use the real one instead of its mathematical model. In this work, the control law design does not consider the actuator dynamics. However, in the final tuning stage of the control gains, the real actuator is included in the hardware-in-the-loop simulations.

Recently, the computer aided control system design (CACSD) has been the subject of focus in control implementation. The CACSD is often named as the rapid control prototyping (RCP) or the hardware-in-the-loop simulations (HILS) (Hanselmann [7,8]). In the RCP, the plant dynamics and/or the control laws are implemented in a digital signal processing board, which allows an easy adjustment of various parameters of the plant and/or the controller. If actual hardware is used as a part of simulation loop, the term ''HILS'' is particularly used. Through the CACSD, the total development time and cost can be much reduced. Also, it is easy to introduce a new component or a new algorithm because the test procedure can be easily repeated.

In this paper, assuming the use of a single acceleration sensor for the quarter-car model and a 16-bit microprocessor, a modified skyhook control with gain scheduling is investigated. Contributions of this paper are: First, a new control-oriented model for the semi-active Macpherson suspension system is derived. Second, a control structure extending the skyhook control and including the estimation of road conditions is suggested. Third, the optimal gains for the ISO road classes and the gain scheduling procedure for estimated roads are developed. Fourth, the procedure for incorporating the actuator dynamics via the hardware-in-the-loop simulations is discussed. One final comment is that four sensors (three vertical sensors and one lateral sensor) for the entire vehicle control are used, but the issues beyond the quarter-car model are not discussed in this paper.

This paper is structured as follows. In Section 2, a new model for the semi-active Macpherson suspension system is derived. In Section 3, the control problem is formulated, the skyhook control is modified, road profiles are characterized, optimal gains for the ISO road classes are determined, the gains for the estimated road and two filters for controller variables are designed. In Section 4, the performance of a controlled semi-active system is evaluated using the hardware-in-the-loop simulations. Conclusions are given in Section 5.

2 Modeling of 1/4 Car: A New Model

A schematic diagram of the Macpherson strut suspension system is shown in Fig. 1. This model admits the rotational motion of the unsprung mass. For the brevity of this paper, the detailed assumptions made for this model are referred to Hong et al. [9]. If the joint between the control arm and the car body is assumed to be a bushing and the mass of the control arm is included, the degree-of-freedom of a 1/4-car system is four. The generalized coordinates in this case are z_s, d, θ_1, and θ_2. However, if the mass of the control arm is neglected and the bushing is assumed to be a pin joint, then the degree-of-freedom becomes two, reducing the generalized coordinates from four to two, z_s and θ as depicted in Fig. 2. In Hong et al. [9], the equations of motion for this model are derived. In this section, the derivation in Hong et al. [9] is modified to fit to the control problem of the semi-active suspension system with a continuously variable damper.

The definitions of the parameters and variables in Fig. 2 are:

Parameters (*Data*): m_s is the sprung mass (453 Kg); m_u is the unsprung mass (36 Kg); k_s is the spring constant of the coil spring (17,658 N/m); k_t is the spring constant of the tire (183,887 N/m); l_A is the distance from O to A (0.66 m); l_B is the distance from O to B (0.34 m); l_C is the length of the control arm (0.37 m); α is the angle between the y-axis and $\overline{OA}$ (74 deg); θ_0 is the angular displacement of the control arm at a static equilibrium point (-2 deg).

Variables: z_s is the vertical displacement of the sprung mass; θ is the angular displacement of the unsprung mass; Δl is the relative displacement in the rattle space, and finally f_s is the control (damping) force generated by the continuously variable damper.

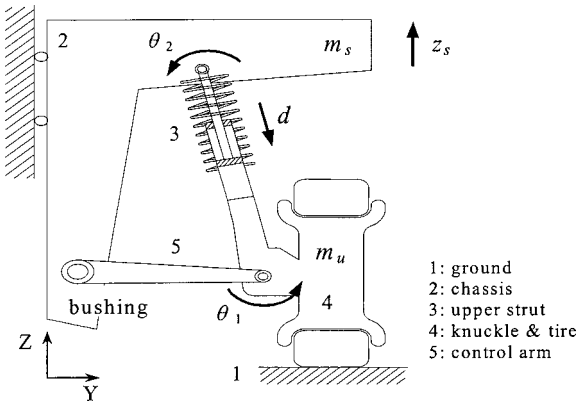

Fig. 1 A schematic diagram of the Macpherson suspension system: 1/4-car model

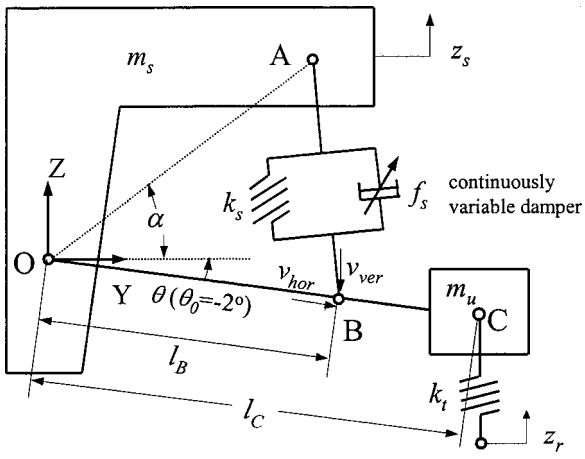

Fig. 2 A new model including the continuously variable damping force

Let T, V, and D denote the kinetic energy, the potential energy and the damping energy of the system, respectively. Then, they are

$$T=\tfrac{1}{2}(m_s+m_u)\dot{z}_s^2+\tfrac{1}{2}m_u l_C^2\dot{\theta}^2+m_u l_C\cos(\theta-\theta_0)\dot{\theta}\cdot\dot{z}_s,$$

$$V=\tfrac{1}{2}k_s\{2a_l-b_l[\cos\alpha'+\cos(\alpha'-\theta)]-2[a_l^2-a_l b_l(\cos\alpha'+\cos(\alpha'-\theta)+b_l^2\cos\alpha'\cos(\alpha'-\theta)]^{1/2}\}+\tfrac{1}{2}k_t\{z_s+l_C[\sin(\theta-\theta_0)-\sin(-\theta_0)-z_r]\},$$

$$D=\frac{1}{2}c_p(\dot{\Delta}l)^2=\frac{c_p b_l^2\sin^2(\alpha'-\theta)\dot{\theta}^2}{8[a_l-b_l\cos(\alpha'-\theta)]},$$

where $a_l=l_A^2+l_B^2$, $b_l=2l_A l_B$, $\alpha'=\alpha+\theta_0$, $c_l=a_l^2-a_l b_l\cos(\alpha')$, and $d_l=a_l b_l-b_l^2\cos(\alpha')$.

For the two generalized coordinates $q_1=z_s$ and $q_2=\theta$, the equations of motion are:

$$(m_s+m_u)\ddot{z}_s+m_u l_C\cos(\theta-\theta_0)\ddot{\theta}-m_u l_C\sin(\theta-\theta_0)\dot{\theta}^2+k_t\{z_s+l_C(\sin(\theta-\theta_0)-\sin(\theta_0))-z_r\}=0, \tag{1}$$

$$m_u l_c^2\ddot{\theta}+m_u l_C\cos(\theta-\theta_0)\ddot{z}_s+k_t l_C\cos(\theta-\theta_0)\{z_s+l_C(\sin(\theta-\theta_0)-\sin(-\theta_0))-z_r\}-\tfrac{1}{2}k_s\sin(\alpha'-\theta)\times\left\{b_l+\frac{d_l}{(c_l-d_l\cos(\alpha'-\theta)^{1/2})}\right\}=-l_B f_s. \tag{2}$$

Remark 1: The semi-active damping force, f_s, in (2) includes both the passive damping force and the control force. However, in Eq. (9) of Hong et al. [9], there appear two explicit terms, i.e., a passive damping coefficient c_p as well as a control input term f_a. The equivalence of (2) and Eq. (9) of Hong et al. [9] is shown as follows: If we set $c_p=0$ and $f_a=f_s$ in (9), (9) and (3) become identical. Also, if we set $c_p=c_s$ and $f_a=0$ in (9), the application of the relationship such that $1/2\cdot\partial D/\partial\dot{\theta}=c_s\dot{\Delta}l\cdot\partial\dot{\Delta}l/\partial\dot{\theta}\cong l_B c_s\dot{\Delta}l=l_B f_s$ to (9) yields (3).

Now, define the state variables as $[x_1\,x_2\,x_3\,x_4]^T=[z_s\,\dot{z}_s\,\theta\,\dot{\theta}]^T$. Then, (1)–(2) can be rewritten as follows:

$$\dot{x}_1=x_2,\qquad \dot{x}_2=f_1(x_1,x_2,x_3,x_4,f_s,z_r),\qquad x_3=x_4,\qquad \dot{x}_4=f_2(x_1,x_2,x_3,x_4,f_s,z_r), \tag{3}$$

where

$$f_1=\frac{1}{g_1(x_3)}\left\{m_u l_C^2\sin(x_3-\theta_0)x_4^2-\frac{1}{2}k_s\times\sin(\alpha'-x_3)\cos(x_3-\theta_0)g_3(x_3)-k_t l_C\sin^2(x_3-\theta_0)z(\cdot)+l_B f_s\cos(x_3-\theta_0)\right\},$$

$$f_2=-\frac{1}{g_2(x_3)}\left\{m_u^2 l_C^2\sin(x_3-\theta_0)\cos(x_3-\theta_0)x_4^2-\tfrac{1}{2}(m_s+m_u)k_s\sin(\alpha'-x_3)g_3(x_3)+m_s k_t l_C\times\cos(x_3-\theta_0)z(\cdot)+(m_s+m_u)l_B f_s\right\},$$

$$g_1(x_3)=m_s l_C+m_u l_C\sin^2(x_3-\theta_0),$$

$$g_2(x_3)=m_s m_u l_C^2+m_u^2 l_C^2\sin^2(x_3-\theta_0),$$

$$g_3(x_3)=b_l+\frac{d_l}{(c_l-d_l\cos(\alpha'-x_3))^{1/2}},$$

$$z(\cdot)=z(x_1,x_2,z_r)=x_1+l_C(\sin(x_3-\theta_0)-\sin(-\theta_0))-z_r.$$

The linearization of (3) at an equilibrium point $x_e=(x_{1e},x_{2e},x_{3e},x_{4e})=(0,0,\theta_0,0)$ yields:

$$\dot{x}(t)=Ax(t)+B_1 f_s+B_2 z_r(t),\quad x(0)=x_0 \tag{4}$$

where

$$A=\left[\begin{array}{cccc}0&1&0&0\\ \frac{\partial f_1}{\partial x_1}&\frac{\partial f_1}{\partial x_2}&\frac{\partial f_1}{\partial x_3}&\frac{\partial f_1}{\partial x_4}\\ 0&0&0&1\\ \frac{\partial f_2}{\partial x_1}&\frac{\partial f_2}{\partial x_2}&\frac{\partial f_2}{\partial x_3}&\frac{\partial f_2}{\partial x_4}\end{array}\right]_{x=x_e}=\left[\begin{array}{cccc}0&1&0&0\\ a_{21}&0&a_{23}&0\\ 0&0&0&1\\ a_{41}&0&a_{43}&0\end{array}\right]=\left[\begin{array}{cccc}0&1&0&0\\ -0.49437&0&21.177&0\\ 0&0&0&1\\ -13796&0&-5105.4&0\end{array}\right],$$

$$B_1=\left[0\ \frac{\partial f_1}{\partial f_s}\ 0\ \frac{\partial f_2}{\partial f_s}\right]_{x=x_e}^T=\left[\begin{array}{c}0\\ \frac{l_B\cos(-\theta_0)}{m_s l_C+m_u l_C\sin^2(-\theta_0)}\\ 0\\ \frac{-(m_s+m_u)l_B}{m_s m_u l_C^2+m_u^2 l_C^2\sin^2(-\theta_0)}\end{array}\right]=\left[\begin{array}{c}0\\ 0.002\\ 0\\ -0.074\end{array}\right],$$

$$B_2=\left[0\ \frac{\partial f_1}{\partial z_r}\ 0\ \frac{\partial f_2}{\partial z_r}\right]_{x=x_e}^T=\left[\begin{array}{c}0\\ \frac{k_t l_C\sin^2(-\theta_0)}{m_s l_C+m_u l_C\sin^2(-\theta_0)}\\ 0\\ \frac{m_s k_t l_C\cos(-\theta_0)}{m_s m_u l_C^2+m_u^2 l_C^2\sin^2(-\theta_0)}\end{array}\right]=\left[\begin{array}{c}0\\ 0.494\\ 0\\ 13796\end{array}\right],$$

and

$$a_{21}=\frac{-k_t l_C\sin^2(-\theta_0)}{m_s l_C+m_u l_C\sin^2(-\theta_0)},$$

$$a_{23}=\frac{1}{\{m_s l_C+m_u l_C \sin^2(-\theta_0)\}^2}\Bigg[\Bigg\{\frac{1}{2}k_s\Bigg(b_l+\frac{d_l}{(c_l-d_l\cos(\alpha'))^{1/2}}\Bigg)\cdot\cos(\alpha'+\theta_0)+\frac{1}{2}k_s\sin\alpha'\cos(-\theta_0)\Bigg(\frac{d_l^2\sin\alpha'}{2(c_l-d_l\cos\alpha')^{3/2}}\Bigg)-k_t l_C^2\sin^2(-\theta_0)\cos(-\theta_0)\Bigg\}\cdot(m_s l_C+m_u l_C\sin^2(-\theta_0))-m_u k_s l_C\sin\alpha'\sin(-\theta_0)\cos^2(-\theta_0)\times\Bigg(b_l+\frac{d_l}{(c_l-d_l\cos\alpha')^{1/2}}\Bigg)\Bigg],$$

$$a_{41}=\frac{-m_s k_t l_C\cos(-\theta_0)}{m_s m_u l_C^2+m_u^2 l_C^2\sin^2(-\theta_0)},$$

$$a_{43}=-\frac{1}{\{m_s m_u l_C^2+m_u^2 l_C^2\sin^2(\theta_0)\}^2}\Bigg[\Bigg\{\frac{1}{2}(m_s+m_u)k_s\cos\alpha'\times\Bigg(b_l+\frac{d_l}{(c_l-d_l\cos\alpha')^{1/2}}\Bigg)-\tfrac{1}{2}(m_s+m_u)k_s\times\sin\alpha'\Bigg(\frac{d_l^2\sin\alpha'}{2(c_l-d_l\cos\alpha')^{3/2}}\Bigg)+m_s k_t l_C^2\cos(-\theta_0)\Bigg\}\cdot(m_s m_u l_C^2+m_u^2 l_C^2\sin^2(-\theta_0))+\frac{1}{2}(m_s+m_u)m_u^2 k_s l_C^2\times\sin\alpha'\sin(-\theta_0)\Bigg(b_l+\frac{d_l}{(c_l-d_l\cos\alpha')^{1/2}}\Bigg)\Bigg].$$

Remark 2: Comparing the linearized Eq. (4) with the conventional model (Yue et al. [6]), in which only the vertical movement of both the sprung and the unsprung masses is considered, the transfer function of the conventional model and that of (4) become identical if $l_B=l_C$, $l_B=l_A\cos\alpha$, and $\theta_0=0$ deg. Therefore, the conventional model is a special case of this new model in the sense that the same transfer function can be achieved by restricting $l_B=l_C$ and $\theta_0=0$. For the detailed comparison, Hong et al. [9] is referred.

Now, because $\ddot{z}_s$ is measured, the output equation by defining $y\equiv\ddot{z}_s$ is derived as follows:

$$y(t)=Cx(t)+D_1 f_s+D_2 z_r, \tag{5}$$

where

$$C=[a_{21}\ \ 0\ \ a_{23}\ \ 0],\quad D_1=\Bigg[\frac{l_B\cos(-\theta_0)}{m_s l_C+m_u l_C\sin^2(-\theta_0)}\Bigg]=[0.002],$$

and

$$D_2=\Bigg[\frac{k_t l_C\sin^2(-\theta_0)}{m_s l_C+m_u l_C\sin^2(-\theta_0)}\Bigg]=[0.494].$$

Remark 3: The variables needed for the computation of control input are the absolute velocity of the sprung mass, $\dot{z}_s$, and the relative velocity of the sprung and unsprung masses $\dot{\Delta}l$. In Section 3.6, both $\dot{z}_s$ and $\dot{\Delta}l$ are filtered from the signal $\ddot{z}_s$ measured. Recall that the use of only one acceleration sensor is assumed in this work. However, during the stage of hardware-in-the-loop simulations of the control laws designed, the following formula, Eq. (5*b*) of Hong et al. [9], can be used.

$$\dot{\Delta}l=\frac{b_l\sin(\alpha'-\theta)\dot{\theta}}{2(a_l-b_l\cos(\alpha'-\theta))^{1/2}}\triangleq f(\theta,\dot{\theta}). \tag{6}$$

Finally, to put the control structure in a feedback form, i.e., the reference signal is $[\dot{z}_s\ \dot{\Delta}l]^T=[0\ 0]^T$ and its error is regulated, a filtered output equation is defined as follows:

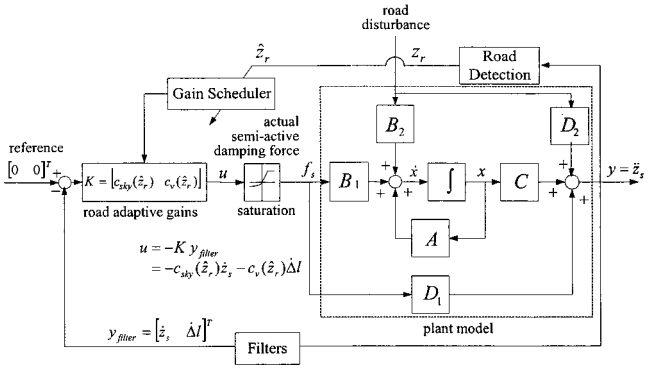

Fig. 3 Control block diagram of the semi-active suspension system: a road adaptive modified skyhook control

$$y_{filter}=\begin{bmatrix}\dot{z}_s\\ \dot{\Delta}l\end{bmatrix}\triangleq\begin{bmatrix}F_1(\ddot{z}_s)\\ F_2(\ddot{z}_s)\end{bmatrix}. \tag{7}$$

Figure 3 depicts the entire control structure, in which the filtering of $\dot{z}_s$ and $\dot{\Delta}l$ from $\ddot{z}_s$ and the road estimation using $\ddot{z}_s$ are clearly emphasized. The road estimation will be discussed in Section 3.5 and the filter design will be discussed in Section 3.6.

3 Control Design: A Road Adaptive Modified Skyhook Control

A number of papers investigating advanced control techniques such as nonlinear adaptive control, preview control, multivariable system decoupling techniques, and robust control have appeared in the literature (Alleyne et al. [10], Yi and Hedrick [11], Alleyne and Hedrick [12], Hac [13], Kim and Yoon [14], El-Demerdash and Crolla [15], Lin and Kanellakopoulos [16], Cherry et al. [17], Choi et al. [18]). However, if a state feedback control strategy is adopted, either sufficient sensors for the whole state variables or an estimate of the state vector is required (Hedrick et al. [19], Yi and Hedrick [20]).

In this paper, the use of only one acceleration sensor for measuring the sprung mass vertical vibrations and a 16-bit microprocessor for implementing the control algorithm is assumed. Therefore, the control law design focuses on the practicality, implementability, and robustness of the algorithm rather than the perfection of performance.

The two control objectives are the improvement of both the ride quality and the handling performance of vehicle. If fixed control gains are used, these two conflicting objectives cannot be achieved. However, by adapting road conditions, i.e., by changing controller gains for various road conditions, both objectives can be achieved.

3.1 Controller Structure. In this paper, as shown in Fig. 3, a modified skyhook control with gain scheduling, in the form of an output feedback control, is proposed. The measured output is $\ddot{z}_s$. The road disturbance is z_r. It is noted that the control law, a modified skyhook control, is not based upon a mathematical model of the plant and therefore the control structure is not a model-based control. However, the mathematical model developed in Section 2 will be used in filtering controller parameters $(\dot{z}_s,\dot{\Delta}l)$ and estimating road conditions $(\hat{z}_r)$. The reason for adopting the structure of Fig. 3 is justified as follows: The entire control problem is to stabilize a two-degree-of-freedom system with a single actuator involving saturation. The actuator dynamics is complicated and its performance is limited. Furthermore, the two conflicting control objectives cannot be satisfied with fixed gains. Therefore, a heuristic algorithm rather than a control algorithm based upon a precise mathematical model is suggested. In this formulation, the desired reference signals are set to $\dot{z}_s=0$ and

$\dot{\Delta l}=0$. Now, after a brief discussion on the control law, the issues related to the road estimation, gain scheduling, and filtering are described in Sections 3.3−3.6, respectively.

1) Ideal Skyhook Control. Among the many control methods developed, the skyhook control introduced by Karnopp et al. [1] is known most effective in terms of the simplicity of the control algorithm. Their original work uses only one inertia damper between the sprung mass and the inertia frame. The skyhook control is applicable for both a semi-active system as well as an active system. However, the original strategy did not pay attention to the unsprung mass vibrations and therefore might deteriorate the handling performance of vehicle due to the excessive vibrations of the unsprung mass. In order to overcome the demerits of the original skyhook control, various modified approaches have been proposed in the literature (Besinger et al. [2], Novak and Valasek [3]).

2) Skyhook-Groundhook Control. The groundhook control by Novak and Valasek [3], which assumes an additional inertia damper between the unsprung mass and the ground, was proposed for the purpose of reducing excessive motion of the unsprung mass. This strategy can compromise the two conflicting criteria, the ride quality and the handling performance of vehicle. From Fig. 2, the control force of the skyhook-groundhook model becomes

$$u=-c_{sky}\dot{z}_s-c_p\dot{\Delta l}-c_{gro}(\dot{z}_s+l_C\dot{\theta}) \tag{8}$$

where c_{sky}, c_p, and c_{gro} are the damping coefficients of the skyhook damper, the passive damper, and the groundhook damper, respectively. However, because the value of $\dot{\theta}$ has to be used, this strategy is not suitable in our case.

3) A Modified Skyhook Control With Gain Scheduling. A modified skyhook control, which proposes the inclusion of a variable damper besides a skyhook damper, can still achieve both control objectives by assigning most appropriate damping coefficients at various road conditions. The following law is proposed:

$$u=-c_{sky}(\hat{z}_r)\dot{z}_s-c_v(\hat{z}_r)\dot{\Delta l} \tag{9}$$

where both the skyhook gain c_{sky} and the variable damper gain c_v depend on the road estimate $\hat{z}_r$. The scheduling of gains is discussed in Section 3.5. Even though the calculation of control input is carried out by (9), the generation of control input should be carried by the variable damper itself. Also, because of saturation, the actual control force from a CVD is limited as follows:

$$f_s=\begin{cases} f_s^*, & \text{if } f_s^*\leqslant u \\ u, & \text{if } f_{s*}<u<f_s^* \\ f_{s*} & \text{if } f_{s*}\geqslant u \end{cases} \tag{10}$$

where f_s^* and f_{s*} denote the maximum and the minimum damping forces available at a given relative velocity. For large control inputs, the actuator saturation would be unavoidable. Therefore, the control performance of a semi-active damper would be less perfect in severe road conditions.

The characteristics of a typical CVD are depicted in Fig. 4. The solid line in the middle section denotes the damping force characteristics of a typical passive damper. The dotted line of highest slope denotes the characteristics for 0 Ampere current input, which is the most hard case. The triangles overlaid on top of the dotted line represent the lookup table values of the maximum damping force. The dotted line of lowest slope denotes the minimum damping force characteristics for 1.6 Ampere current input. Again, the squares denote the lookup table values of the minimum damping force. The damping forces in the extension region (the first quadrant in Fig. 4) are larger than those in the compression region (the third quadrant).

3.2 Current Generation. The damping force generated in a hydraulic-type semi-active damper depends on two things: the size of valve opening, i.e., the current input to the solenoid valve, and the relative velocity in the rattle space. To determine the current input to the solenoid valve, it is necessary to know the damping force characteristics of the valve versus the current input at a given relative velocity. For this, two approaches can be pursued. One is an analytic approach, which investigates a mathematical expression for the entire hydraulic system including the cylinder and valve dynamics. However, the mechanism of a semi-active damper is very complicated and the damping force characteristics in the expansion and compression strokes are different because the volumes of compression and reaction chambers are different and some valves allow the fluid to flow only in one direction. It is also difficult to measure the parameter values and furthermore the viscosity of oil and gas mixture may vary in temperature and time. Another approach is an experimental approach, which is more or less straightforward. The damping forces for various input currents for a specific relative velocity can be measured in a test rig. In this paper, the experimental approach is adopted.

The experimental data can be either tabulated as a look-up table or approximated as a polynomial equation by using the least squares method. After dividing the relative velocity range into four different sections, the polynomial equations made for individual sections are tabulated in Table 1.

As far as the final results are concerned, as seen in Fig. 4 where the number of cases for the lookup table is $N_p=51$, there is not much difference between these two approaches. However, a smaller access time is possible with the polynomial approach. This is very important because the entire control algorithm should be coded in a 16-bit microprocessor. Figure 5 compares the access time of the two methods for the relative velocity range within ± 1.4 m/s. It is seen that the access time to the polynomial equation is constant, but the access time to use the look-up table in-

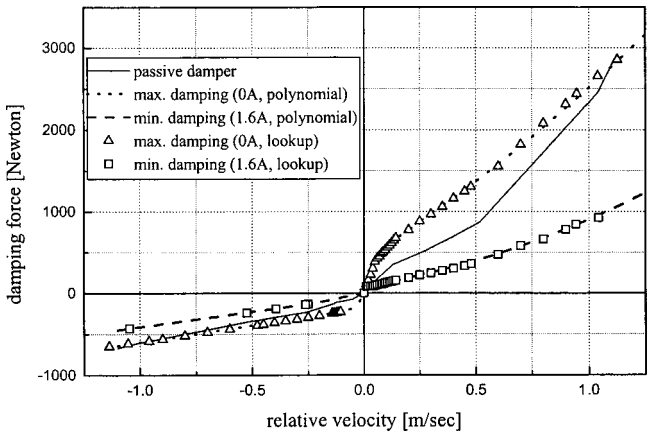

Fig. 4 Damping force characteristics of a typical CVD: comparison between lookup table and polynomial

Table 1 Polynomial representation of maximum/minimum damping forces

	Maximum Damping Force [N]	Minimum Damping Force [N]
$0.25<\dot{\Delta l}$	$440+1650\,\dot{\Delta l}+420\,\dot{\Delta l}^2$	$95+405\,\dot{\Delta l}+402\,\dot{\Delta l}^2$
$0<\dot{\Delta l}<0.25$	$8500\,\dot{\Delta l}-36500\,\dot{\Delta l}^2+66450\,\dot{\Delta l}^3$	$37+1504\,\dot{\Delta l}-7284\,\dot{\Delta l}^2+17164\,\dot{\Delta l}^3$
$-0.1<\dot{\Delta l}<0$	$6700\,\dot{\Delta l}+78000\,\dot{\Delta l}^2+340000\,\dot{\Delta l}^3$	$530\,\dot{\Delta l}$
$\dot{\Delta l}<-0.1$	$410\,\dot{\Delta l}-190$	$370\,\dot{\Delta l}-16$

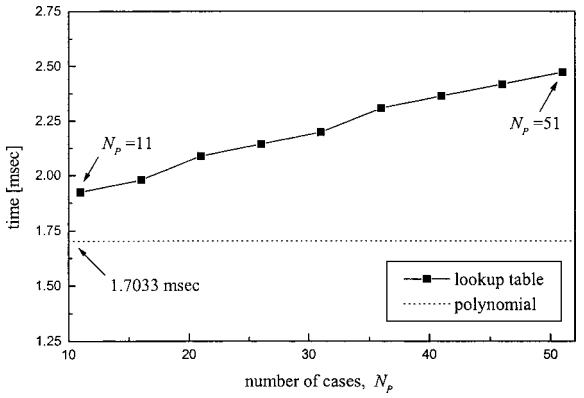

Fig. 5 Access time comparison: lookup table and polynomial

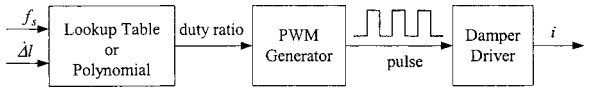

Fig. 6 Current generation

Table 2 ISO road classes

Road classes	Roughness coefficient κ_i [$m^2 \cdot$ (cycles/m)]	
	Range	Average
A (Very good)	2×10^{-6} - 8×10^{-6}	4×10^{-6}
B (Good)	8×10^{-6} - 32×10^{-6}	16×10^{-6}
C (Average)	32×10^{-6} - 128×10^{-6}	64×10^{-6}
D (Poor)	128×10^{-6} - 512×10^{-6}	256×10^{-6}
E (Very poor)	512×10^{-6} - 1048×10^{-6}	1024×10^{-6}

creases as the number of cases increases. This is because each case accesses 1000 data. In this work, the polynomial approach is adopted.

As seen in Fig. 6, the transformation algorithm block determines the duty ratio of a PWM generator by taking two inputs, the desired control force and the relative velocity of the rattle space. In our case, the duty ratios that correspond to 1.6 Ampere and 0 Ampere are set to 0.4 and 0, respectively. The natural frequency of the solenoid valve is about 300 Hz.

3.3 Road Profiles. In this section, the ISO road profiles for the purpose of gain scheduling are described. The mean square displacement spectral density of a track, along the length of a (single-sided) road surface, defined by the ISO is

$$S_i(\Omega)=\kappa_i(\Omega/\Omega_c)^{-N}, \quad N=\begin{cases}2, & \text{if } \Omega\leqslant\Omega_c\\ 1.5, & \text{if } \Omega>\Omega_c\end{cases} \tag{11}$$

where Ω is the wave number in cycles/m, $\Omega_c=1/2\pi$ is the critical wave number, κ_i is the roughness coefficient, $i=A,B,\ldots,E$ denote various road classes, and N is a dimensionless exponent (Robson, [21], Sharp and Crolla, [22]). Table 2 shows five ISO road classes.

For a given vehicle speed, (12) can be converted to a frequency domain characterization of a road by utilizing the relationship between a wave number and a frequency such that $f=V\cdot\Omega$, where f is the excitation frequency in Hz and V is the speed of a vehicle in m/sec, as follows:

$$S_i(f)=\kappa_i V^{N-1}f^{-N}, \quad N=\begin{cases}2, & \text{if } \Omega\leqslant\Omega_c\\ 1.5, & \text{if } \Omega>\Omega_c\end{cases}. \tag{12}$$

Note that once the vehicle speed V is fixed, the following relationship holds (also see Table 2).

$$S_{i+1}(f)=4S_i(f), \quad \text{for both } N=1.5 \quad \text{and} \quad 2. \tag{13}$$

On the other hand, for a constant κ_i, the relationship between the spectral density of speed aV and that of speed V becomes

$$S_a(f)\triangleq\kappa_i(aV)^{N-1}f^{-N}=a^{N-1}\kappa_i V^{N-1}f^{-N}=a^{N-1}S_i(f). \tag{14}$$

Therefore, comparing (13) and (14) for $a^{N-1}=4$, the spectral density on the ISO ith road at speed aV is identical to the spectral density on the ISO $(i+1)$th road at speed V. If $1<a^{N-1}\leqslant4$, this can be considered as the case that the vehicle runs on a road of roughness between the ISO ith class and the ISO $(i+1)$th class at speed V. Similarly, if $a^{N-1}>4$, this corresponds to the case that the vehicle runs on a road of roughness higher that the ISO $(i+1)$th class at speed V.

All these observations suggest that once the optimal gains for all ISO roads for a fixed speed are determined, then the gain for an arbitrary speed can be interpolated from the optimal gains for the standard ISO roads. Therefore, it is not necessary to make a 2-dimensional lookup table, for the purpose of gain scheduling, for the vehicle speed and the road classes. Instead, a 1-dimensional lookup table for the road roughness is sufficient. In this work, $V=60$ Km/h is used.

3.4 Optimal Gains for the ISO Roads. The variations of c_{sky} and c_v in (9) affect both the ride quality and the road holding ability of vehicle. Figure 7 shows the conflicting behavior between two criteria for various input conditions (simulation results), in which the ISO C-class road and a vehicle speed of 60 km/h are used. All plots are generated using the suspension model developed in Section 2. The big circle marked at 0.86 m/sec^2 in the x-axis and 910 Newton in the y-axis indicates the characteristics of the passive damper in Fig. 4. Because the CVD in Fig. 4 has saturation, its performance is limited to the inside of the dotted rectangle. All curves extending outside the dotted rectangle are obtained by assuming no saturation. As magnified in the upper right corner, if c_{sky} is increased while fixing c_v, the body acceleration decreases but the dynamic tire force increases. Also, if c_v is increased while fixing c_{sky}, the tire force decreases but the body acceleration increases.

Now, the procedure for determining optimal gains for various ISO road classes are discussed. Assume that N_d-data of the dynamic tire force and body acceleration, i.e., $TF(i)$, $BA(i)$, $i=1,\ldots,N_d$, have been collected for each ISO road input. Then, the optimal coefficients are determined using the following criterion.

$$(c_{sky},c_v)_{optimal}=\min_i\left\{\sqrt{\left[w_t(z_r)\cdot\frac{TF(i)-TF_{\min}}{TF_{\max}-TF_{\min}}\right]^2+\left[w_a(z_r)\cdot\frac{BA(i)-BA_{\min}}{BA_{\max}-BA_{\min}}\right]^2}\right\}_{i=1}^{N_d} \tag{15}$$

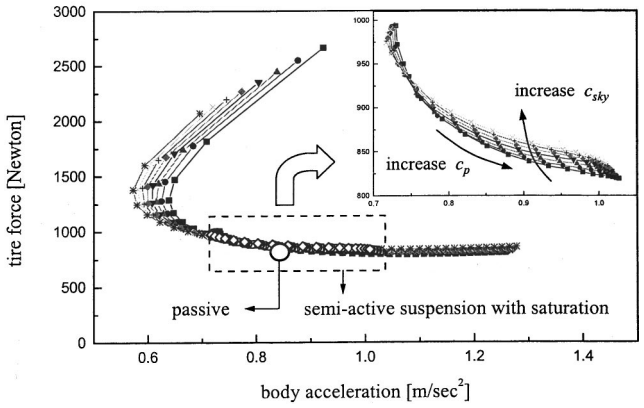

Fig. 7 Conflicting behavior between the ride comfort and the handling performance of vehicle

where TF and BA denote the RMS values of the dynamic tire force and the body acceleration; $w_a(z_r)$ and $w_t(z_r)$ are two weighting factors, respectively. The selection of the weighting factors is subjective, but the rougher the road is, the larger $w_t(z_r)$ is suggested. It is also noted that the gains should be selected in such a way that the dynamic tire force is smaller than the static tire force. Finally, the optimal gains determined for all ISO roads are tabulated in Table 3.

3.5 Road Detection and Gain Tuning. In this section, using the data $\ddot{z}_s$ measured, the estimation of road roughness and the determination of the controller gain for the estimated road are described. The transfer function from $z_r(s)$ to $\ddot{z}_s(s)$ is derived from (4) and (5) as follows:

$$G_{rs}(s)\triangleq\frac{\ddot{z}_s(s)}{z_r(s)}=C'(sI-A')^{-1}B_2+D_2$$

$$=\frac{0.5s^4+17212.4s^3+317325s^2-11.5s-212.6}{s^4+45.7s^3+509765s^2+17212.4s+317359} \tag{16}$$

where $A'=A+B_1H$, $C'=C+D_1H$, (A,B_2,C,D_2) are from (4)–(5), and H satisfies $f_s=c_p\dot{\Delta l}\cong Hx$, where $H\triangleq c_p[0\ 0\ \partial\dot{\Delta l}/\partial\theta\ \partial\dot{\Delta l}/\partial\dot{\theta}]_{(0,0,\theta_0,0)}$. It is noted that H has been introduced to avoid possible roots on the imaginary axis. In this work, $H=[0\ 0\ 0\ 614]$ has been used. Therefore, using the transfer function above, the road input can be estimated as follows:

$$z_r(s)=\frac{40\pi}{s+40\pi}\cdot G_{rs}^{-1}(s)\cdot\ddot{z}_s(s) \tag{17}$$

where a low-pass filter of cutoff frequency 20 Hz has been added to enhance the stability of the filter.

Now, the gain selection for the estimated road is described. A real road contains various frequency components. But, the dominant components measured in the sprung mass will be the resonance frequencies of the suspension system. The eigenvalues of A' are $-1.49\pm j7.60$ and $-21.38\pm j66.73$, which correspond to the resonance frequencies of the sprung and unsprung masses at $f_{bn}=1.23$ Hz and $f_{wn}=11.15$ Hz, respectively.

Now, let ΔT and N_s be the sampling time and the number of data collected from (17), respectively. In this work, $N_s=50$ and $\Delta T=10$ msec are used. Let the discrete Fourier transform of $Z_r=(z_r(0),z_r(1),\ldots,z_r(N_s-1))$ be

$$\overline{Z}_{rk}=\sum_{m=0}^{N_s-1}z_r(m)\cdot e^{-j(2\pi km/N_s)}=A_{rk}+jB_{rk},\quad k=0,1,\ldots,N_s-1 \tag{18}$$

where

$$A_{rk}=\frac{2}{N_s}\sum_{m=0}^{N_s-1}z_r(m)\cdot\cos\frac{2\pi km}{N_s},\quad k=1,2,\ldots,\frac{N_s}{2}$$

$$B_{rk}=\frac{2}{N_s}\sum_{m=0}^{N_s-1}z_r(m)\cdot\sin\frac{2\pi km}{N_s},\quad k=0,1,\ldots,\frac{N_s}{2}-1.$$

Because $N_s=50$ and $\Delta T=10$, the frequency resolution becomes 2 Hz. Therefore, 2 Hz and 10 Hz are assumed to be the resonance frequencies of the suspension system approximating 1.23 Hz and 11.15 Hz, respectively. For a better approximation, a smaller sampling frequency may be used. But, the selection of sampling time and data size is related to the microprocessor used. Let $S(f_{bn})$ and $S(f_{wn})$ denote the magnitudes at frequencies f_{bn} and f_{wn}, respectively, i.e.,

$$S(f_{bn})=\sqrt{A_{r1}^2+B_{r1}^2}\quad\text{and}\quad S(f_{wn})=\sqrt{A_{r5}^2+B_{r5}^2}. \tag{19}$$

While $S(f_{bn})$ in (19) can be directly used as a criterion for gain selection, $S(f_{wn})$ should be converted to the equivalent energy level at the sprung mass resonance frequency as follows:

$$S(f'_{bn})=\frac{S_i(f_{bn})}{S_i(f_{wn})}\cdot S(f_{wn})=\frac{(f_{bn})^{-N_b}}{(f_{wn})^{-N_w}}\cdot S(f_{wn}) \tag{20}$$

where

$$(N_b,N_w)=\begin{cases}(1.5,1.5), & \text{for } 2\pi\cdot f_{bn}>V\\ (2,1.5), & \text{for } 2\pi\cdot f_{bn}\leqq V<2\pi\cdot f_{wn}.\\ (2,2), & \text{for } 2\pi\cdot f_{wn}\leqq V\end{cases}$$

In deriving (20), (12) has been utilized. Finally, the bigger value between two is selected as follows:

$$S(f)=\max\{S(f_{bn}),S(f'_{bn})\}. \tag{21}$$

Figure 8 shows estimation of three types of the ISO roads, using the scheme in this section. It is seen that the convergence requires at least 0.5 second to collect 50 data points.

Table 3 Optimal gains for the ISO road classes

Road classes	Weight factors $(w_a,\ w_t)$	Optimal gains $(c_{sky},\ c_p)$
A (Very good): $S_A(f)$	(0.8, 0.2)	(2500, 1200)
B (Good): $S_B(f)$	(0.7, 0.3)	(1500, 1400)
C (Average): $S_C(f)$	(0.6, 0.4)	(1000, 1600)
D (Poor): $S_D(f)$	(0.4, 0.6)	(500, 2000)
E (Very poor): $S_E(f)$	(0.3, 0.7)	(0, 2800)

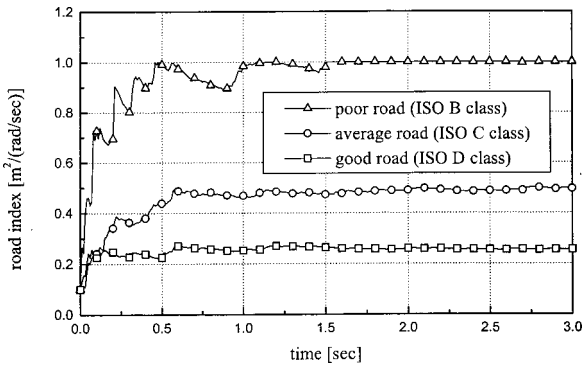

Fig. 8 Estimation of the ISO B, C, and D road classes (simulation results): sampling time $\Delta T=10$ msec

Finally, let $S(f)$ satisfy $S_i(f_{bn}) < S(f) \leqslant S_{i+1}(f_{bn})$, where $S_i(f_{bn})$ and $S_{i+1}(f_{bn})$ are the magnitudes of ISO ith and $(i+1)$th roads, respectively. Then, the control gain g^o for the current road estimated is interpolated logarithmically by using the predetermined optimal gains for the ISO roads as follows:

$$g^o = \frac{\log\left(\frac{S_{i+1}(f_{bn})}{S(f)}\right) g_i^o + \log\left(\frac{S(f)}{S_i(f_{bn})}\right) g_{i+1}^o}{\log S_{i+1}(f_{bn}) - \log S_i(f_{bn})} \tag{22}$$

where g_i^o and g_{i+1}^o are the optimal gains for ISO ith and $(i+1)$th roads, respectively.

3.6 Filter Design. In this section, two filters for estimating the absolute velocity of the sprung mass and the relative velocity of the sprung and unsprung masses are designed. It is also remarked that even though the measurement of θ or $\dot{\theta}$ is possible, an estimation method is preferred considering the cost for extra sensors.

1) Absolute Velocity of the Sprung Mass. The filter to estimate the absolute velocity from the acceleration data of the sprung mass is suggested as follows:

$$\dot{z}_s = F_1(\ddot{z}_s) = \frac{s}{s^2 + 2\zeta\omega_n s + \omega_n^2} \ddot{z}_s \tag{23}$$

where $\zeta = 0.707$ and $\omega_n = 0.1$ Hz. Equation (23) performs as a differentiator below 0.1 Hz and as an integrator above 0.1 Hz. Consequently, this filter will provides a satisfactory absolute velocity of the sprung mass by excluding a possible DC offset.

2) Relative Velocity of the Sprung and Unsprung Masses. The relative velocity of two masses is estimated using the model of suspension dynamics. Assume that $\theta_0 = 0$ and θ is sufficiently small. Then, the following approximations hold:

$$\nu_{hor} \cong 0, \quad \dot{z}_u \cong \dot{z}_s + l_C\dot{\theta}, \quad \dot{\theta} \cong \frac{1}{l_C}(\dot{z}_u - \dot{z}_s)$$

and

$$\dot{\Delta l} \cong -l_B\dot{\theta} = \frac{l_B}{l_C}(\dot{z}_s - \dot{z}_u). \tag{24}$$

Therefore, the relative velocity from measurement data is filtered as follows:

$$\dot{\Delta l} = F_2(\ddot{z}_s) = \frac{l_B}{l_C} \cdot \frac{(\dot{z}_s - \dot{z}_u)}{\ddot{z}_s} \ddot{z}_s = -\frac{l_B}{l_C} \cdot \frac{m_s s}{c_p s + k_s} \cdot \frac{1}{1+\tau s} \ddot{z}_s \tag{25}$$

where m_s, c_p, and k_s are the suspension parameters. It is noted that a low pass filter $1/(1+\tau s)$ has been added for eliminating noises, where $\tau = 1/2\zeta\omega_l$, $\zeta = 0.707$, and $\omega_l = 15 \sim 20$ Hz.

4 Hardware-in-the-Loop Simulations

The CVD unit has been used for the hardware-in-the-simulations (HILS). The purpose of the HILS is to consider the actuator dynamics neglected during the stages of modeling and control system design. Therefore, the nonlinear characteristics of the damping force together with the time-delay and the neglected dynamics of the solenoid valve can be fully incorporated during the HILS. Figure 9 shows the configuration for the HILS. MATLAB/SIMULINK (MathWorks Inc.) is used as a computer-aided control system tool, i.e., a programming environment, and a dSPACE board (digital signal processor board of dSPACE GmbH Inc.) is used as a rapid control prototyping tool for implementing the plant dynamics and control laws.

The input current, generated by the PWM voltage signal from TMS320P14, changes the damping force of the CVD. The relative velocity of the sprung and unsprung masses is made by the MTS test rig, which consists of a hydraulic actuator, a loadcell, a LVDT, etc. The procedure for the HILS is summarized as follows:

1 The control algorithm is first of all designed off-line using MATLAB/SIMULINK.

2 Using the Real-Time-Workshop, a C-code of the control algorithm from its block diagram form is generated. The C-code is again downloaded to the target DSP board using the Real-Time-Interface. Therefore, the dynamic models developed can be reused easily for the HILS.

3 The PWM voltage signal related to the damping force and the relative displacement (stroke) calculated from the dynamic model in the computer are transmitted to the damper drive unit and the MTS control unit, respectively, through D/A converters.

4 The damper drive unit transforms the PWM voltage signal into a current signal from 0 Ampere to 1.6 Ampere and supplies the current signal to the CVD. The PWM voltage signal has 2 kHz carrier frequency and the duty ratio of the PWM voltage signal

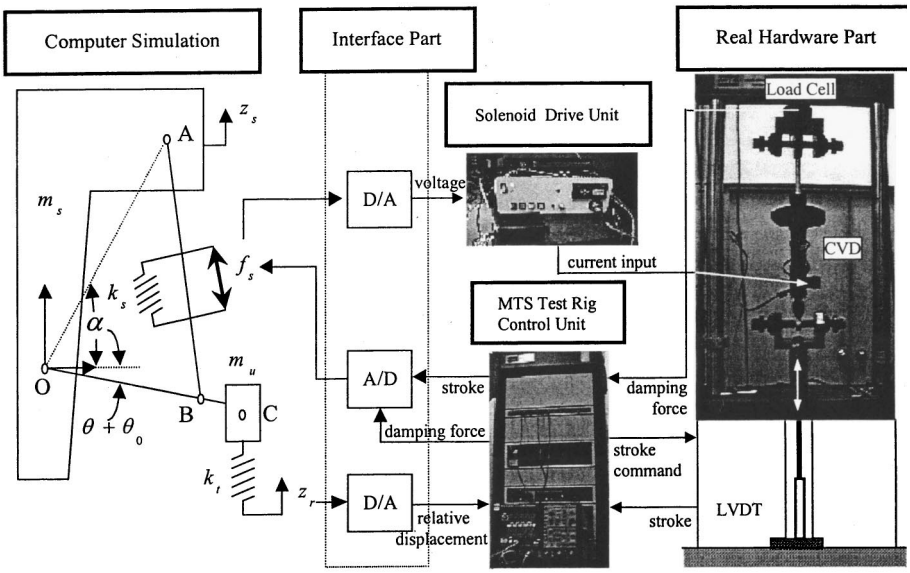

Fig. 9 Configuration for the hardware-in-the-loop simulations

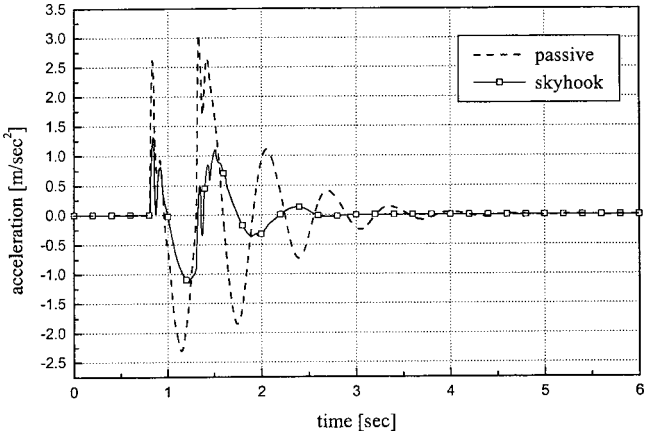

Fig. 10 Vertical acceleration comparison between a passive damper and a CVD with the modified skyhook control (experimental results): 1 Hz speed bump

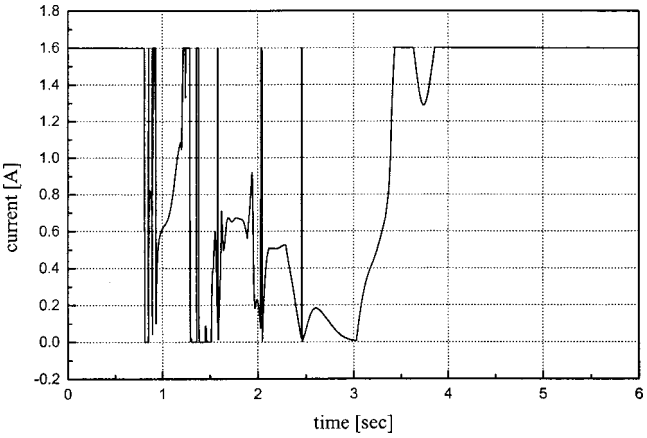

Fig. 11 Current input applied to the CVD in Fig. 10: 1 Hz speed bump

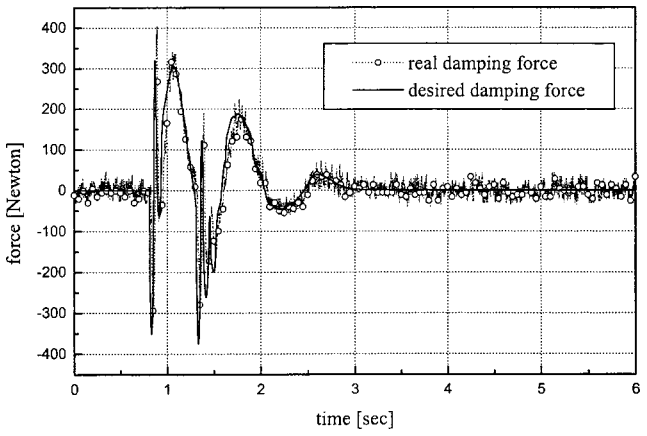

Fig. 12 Tracking performance of the desired damping force: 1 Hz speed bump

corresponding to 1.6 Ampere is 0.4. The MTS control unit excites the hydraulic actuator according to the relative displacement command.

5 The damping force of the CVD and the relative displacement are measured using a loadcell and a LVDT, respectively, and transferred to the dynamic model in the computer. By varying the control parameters in real time, the procedures 3–5 can be repeated.

The sampling time is set to 0.01 s. This time step should be larger than the combined time of the calculation time of the plant dynamics and the input-output communication time between the external devices. In experiments when the actual calculation time was larger than the step size, small oscillations had occurred in a valve of the hydraulic actuator. If these oscillations are delivered to the CVD, it will be difficult to measure the exact damping force from the loadcell. Hence, it may affect the stability of the complete control system.

Finally, using the speed bumper of 1 Hz, the vertical accelerations of the sprung mass for a passive damper and a semi-active damper are compared in Fig. 10. The modified skyhook controller with $c_{sky}=2000\,\mathrm{N\cdot s/m}$, $c_v=1960\,\mathrm{N\cdot s/m}$ shows a smaller overshoot and a less settling time compared to the passive damper. Figure 11 shows the current input applied to the CVD. It is shown that 0 Ampere current input was applied to the periods of high vertical accelerations. The force tracking performance of the semi-active damper is depicted in Fig. 12.

5 Conclusions

In this paper, a new control-oriented model and a road-adaptive control scheme for the semi-active Macpherson suspension system were investigated. The new model incorporates the rotational motion of the unsprung mass, giving a better description for the plant dynamics and keeping the degree-of-freedom of the plant model by two. Upon the requirement of using only one acceleration sensor, a modified skyhook control with gain scheduling was developed. The road estimation and the control variables estimation are based upon the linearized model developed. Considering the complexity of the hydraulic semi-active damper, the actuator dynamics has been incorporated during the hardware-in-the-loop simulations. It was demonstrated that the semi-active system could achieve a competitive control performance by adopting the road adaptive control laws. Because the control law design, the road estimation method, the gain scheduling strategy, and the hardware-in-the-loop simulation method developed in this paper are not restricted to a particular suspension system, the entire strategy can be extended to any semi-active system including the ER damper and the MR damper.

Acknowledgments

This work was supported in part by the Korea Research Foundation under Grant KRF-2000-EA0096. The second author was supported in part by the Brain Korea 21 Program of the Ministry of Education and Human Resources, Korea.

References

[1] Karnopp, D. C., Crosby, M. J., and Harwood, R. A., 1974, "Vibration Control Using Semi-Active Force Generators," ASME J. Eng. Ind., **96**, No. 2, pp. 619–626.
[2] Besinger, F. H., Cebon, D., and Cole, D. J., 1995, "Force Control of a Semi-Active Damper," Veh. Syst. Dyn., **24**, pp. 695–723.
[3] Novak, M., and Valasek, M., 1996, "A New Concept of Semi-Active Control of Trucks Suspension," *Proc. of AVEC 96, International Symposium on Advanced Vehicle Control*, Aachen University of Technology, pp. 141–151.
[4] Jonsson, M., 1991, "Simulation of Dynamical Behavior of a Front Wheel Suspension," Veh. Syst. Dyn., **20**, pp. 269–281.
[5] Stensson, A., Asplund, C., and Karlsson, L., 1994, "The Nonlinear Behavior of a Macpherson Strut Wheel Suspension," Veh. Syst. Dyn., **23**, pp. 85–106.
[6] Yue, C., Butsuen, T., and Hedrick, J. K., 1989, "Alternative Control Laws for Automotive Active Suspension," ASME J. Dyn. Syst., Meas., Control, **111**, pp. 286–291.
[7] Hanselmann, H., 1996, "Hardware-in-the-loop Simulation Testing and its Integration into a CACSD Toolset," *The IEEE International Symposium on Computer Aided Control System Design*, Dearborn, MI, pp. 152–156.
[8] Hanselmann, H., 1996, "Automotive Control: From Concept to Experiment to Product," *The IEEE International Symposium on Computer Aided Control System Design*, Dearborn, MI, pp. 129–134.
[9] Hong, K. S., Jeon, D. S., Yoo, W. S., Sunwoo, H., Shin, S. Y., Kim, C. M., and

Park, B. S., 1999, ''A New Model and an Optimal Pole-placement Control of the Macpherson Suspension System,'' *SAE International Congress and Exposition*, Detroit, MI, SAE paper No. 1999–01–1331, pp. 267–276.
[10] Alleyne, A., Neuhaus, P. D., and Hedrick, J. K., 1993, ''Application of Nonlinear Control Theory to Electronically Controlled Suspensions,'' Veh. Syst. Dyn., **22**, pp. 309–320.
[11] Yi, K., and Hedrick, J. K., 1993, ''Dynamic Tire Force Control by Semi-Active Suspension,'' ASME J. Dyn. Syst., Meas., Control, **115**, No. 3, pp. 465–474.
[12] Alleyne, A., and Hedrick, J. K., 1995, ''Nonlinear Adaptive Control of Active Suspensions,'' IEEE Trans. Control Syst. Technol., **3**, No. 1, pp. 94–101.
[13] Hac, A, 1995, ''Decentralized Control of Active Vehicle Suspension with Preview,'' ASME J. Dyn. Syst., Meas., Control, **117**, No. 4, pp. 478–483.
[14] Kim, H., and Yoon, Y. S., 1995, ''Semi-Active Suspension with Preview Using a Frequency-Shaped Performance Index,'' Veh. Syst. Dyn., **24**, pp. 759–780.
[15] El-Demerdash, S. M., and Crolla, D. A., 1996, ''Hydro-pneumatic Slow-active Suspension with Preview Control,'' Veh. Syst. Dyn., **25**, pp. 369–386.
[16] Lin, J. S., and Kanellakopoulos, I., 1997, ''Nonlinear Design of Active Suspensions,'' IEEE Control Syst. Mag., **17**, No. 3, pp. 45–59.
[17] Cherry, A. S., Jones, R. P., and Potter, T. E. C., 1999, ''The Use of Multibody System Modeling and Multivariable System Decoupling Technique in Vehicle Ride Control,'' ASME J. Dyn. Syst., Meas., Control, **121**, No. 3, pp. 479–486.
[18] Choi, S. B., Choi, Y. T., and Park, D. W., 2000, ''A Sliding Mode Control of a Full-Car Electrorheological Suspension System via Hardware-in-the-Loop Simulation,'' ASME J. Dyn. Syst., Meas., Control, **122**, No. 2, pp. 114–121.
[19] Hedrick, J. K., Rajamani, R., and Yi, K., 1994, ''Observer Design for Electronic Suspension Applications,'' Veh. Syst. Dyn., **23**, pp. 413–440.
[20] Yi, K., and Hedrick, J. K., 1995, ''Observer-Based Identification of Nonlinear System Parameters,'' ASME J. Dyn. Syst., Meas., Control, **117**, No. 2, pp. 175–182.
[21] Robson, J. D., 1979, ''Road Surface Description and Vehicle Response,'' Int. J. Veh. Des., **1**, No. 1, pp. 25–35.
[22] Sharp, R. S., and Crolla, D. A., 1987, ''Road Vehicle Suspension System Design—a Review,'' Veh. Syst. Dyn., **16**, pp. 167–192.